HYDROLOGICAL PROCESSES, VOL. 10, 1527–1543 (1996)

# INVESTIGATION OF INFILTRATION CHARACTERISTICS AND DEBRIS FLOW INITIATION CONDITIONS IN DEBRIS FLOW SOURCE AREAS USING A RAINFALL SIMULATOR

H. M. BLIJENBERG, P. J. DE GRAAF, M. R. HENDRIKS,
J. F. DE RUITER AND A. A. A. VAN TETERING

*The Netherlands Centre for Geo-ecological Research, Geomorphological Research Group, Utrecht University, Department of Physical Geography, PO Box 80115, 3508 TC Utrecht, The Netherlands*

## ABSTRACT

Rainfall was simulated on unconfined plots on regolith in debris flow source areas using a portable simulator. In total, 351 simulations were carried out on steep slopes (27–54°) with rainfall intensities of 28–291 mm/h. From these rainfall simulations the infiltration parameters sorptivity ($S$) and steady-state infiltration capacity ($K$) of the regolith, and a threshold for the occurrence of micro-scale mass movements, were obtained. Two evaluation methods were used to obtain the infiltration parameters $K$ and $S$. The 'infiltration envelope' method uses rainfall intensity and time to ponding from multiple tests and fits an infiltration envelope through the data from which $K$ and $S$ can be obtained. The 'constant runoff' method uses rainfall intensity and overland flow intensity to calculate $K$, after which $S$ can be calculated in several ways by using time to ponding. The constant runoff method produced $K$ values of 16·6–128 mm/h, which usually show a log-normal distribution. $K$ values depend on the regolith parent material and rainfall intensity. Using this method, $S$ values are 0·088–0·381 cm/min$^{1/2}$. The infiltration envelope method produced $K$ values of 9·8–131 mm/h and $S$ values of 0·14–0·32 cm/min$^{1/2}$. It can be argued that both methods overestimate $K$ as well as $S$, but quantitative relations between measured/calculated and actual values of $K$ and $S$ have not yet been obtained. At high rainfall intensities, typically 100 mm/h or more, micro-scale mass movements sometimes occur. A lower threshold curve for the occurrence of these micro-scale mass movements has been constructed. It is a function of both slope angle and rainfall intensity. The micro-scale mass movements could play an important part in the initiation of debris flows in the study area, possibly by delivering sediment to overland flow. On the very steep slopes, the sediment-rich overland flow can easily mobilize coarse material.

KEY WORDS rainfall simulation; infiltration; steady-state infiltration capacity; sorptivity; infiltration envelope; micro-scale mass movement; debris flow initiation

## INTRODUCTION

In 1991 the project 'The Temporal Analysis of Debris Flows in an Alpine Environment' was started at Utrecht University. Initially it was financed by EPOCH. The final aim of the project is to forecast the initiation and frequency of debris flows, based on precipitation characteristics on the one hand and on morphological and hydrological characteristics of the source areas of debris flows on the other.

In the study area (Figure 1) debris flows are usually triggered by overland flow produced by high-intensity rain storms. Therefore, part of the project is to investigate the interaction between rainfall and the soil surface. This paper discusses the infiltration characteristics of regolith material and the dependence of micro-scale mass movements on rainfall intensity and slope gradient.

## DEBRIS FLOW INITIATION AND INFILTRATION

Debris flows are defined as rapid mass movements of granular solids, water and air, moving as a viscous flow (Varnes, 1978). Within the project, attention is focused on small-scale hillslope debris flows. Innes (1983) defined small-scale debris flows as debris flows with a deposit volume of $1–10^3$ m$^3$. Hillslope debris

CCC 0885–6087/96/111527–17

*Received 13 March 1995*
*Accepted 14 July 1995*

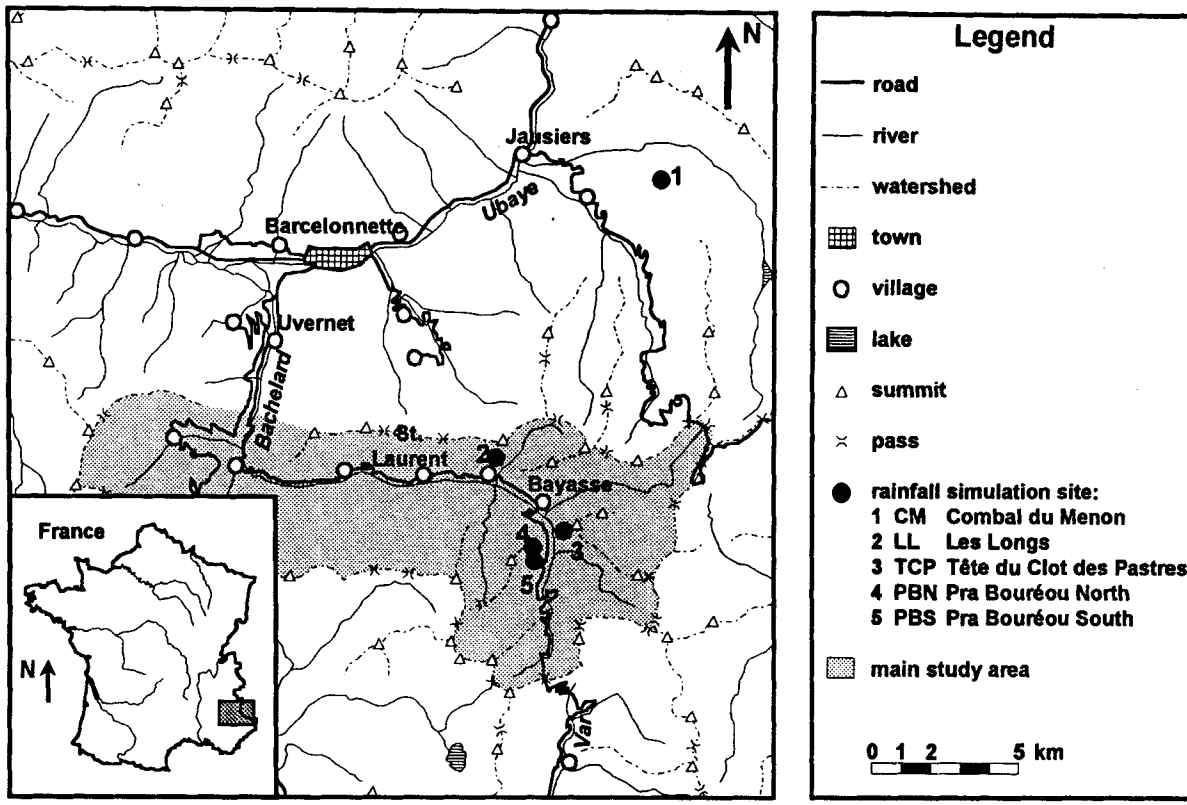


Figure 1. Location of the study area in south-east France

flows are those that occur on mountain slopes and do not continue their movement when they reach the valley floor (Brunsden, 1979).

Prerequisites for the occurrence of debris flows are steep slopes, available regolith, high pore water pressures and a loss of consistency of the material after the initiation of movement. Debris flows can be initiated in many different ways. Landslides can transform into debris flows by dilatancy or liquefaction during movement (Johnson and Rodine, 1984; Johnson and Rahn, 1970). Takahashi (1978; 1980; 1981) describes the spontaneous initiation of a debris flow by dilatancy when a water film of a certain thickness appears at the surface of a saturated body of debris in a channel. Other possible mechanisms include spontaneous liquefaction, damming of water behind debris dams (Costa, 1984) and the 'firehose effect' caused by the impact of a high-speed stream of water (Johnson and Rodine, 1984).

Although external forces, such as vibrations caused by earthquakes or impact forces caused by avalanches (Bovis and Dagg, 1987) can initiate debris flows, usually an increase in pore water pressures caused by a supply of water to the material provides the trigger mechanism. Rainfall and snowmelt are the most frequent water suppliers.

Caine (1980) has found a lower limit of rainfall intensity for the triggering of debris flows and shallow landslides. According to Caine, debris flows are unlikely to occur if

$$i_r < 14{\cdot}82D^{-0{\cdot}39} \tag{1}$$

where $i_r$ = rainfall intensity (mm/h) and $D$ = rainfall duration (h).

In the study area high-intensity short-duration rain storms trigger most debris flows; according to eye-witness observations 5–10 minutes of 50–100 mm/h rainfall intensity are sufficient for debris flow initiation (Van Asch and Van Steijn, 1991). Long-duration low-intensity rainfall and snowmelt hardly ever produce debris flows in the study area.

During high-intensity rain storms infiltration excess overland flow (Hortonian overland flow) will be produced on bare bedrock slopes and on slopes covered with fine-grained regolith. Raindrop impact and fluid flow stresses may detach soil particles, which can then be transported by the overland flow. This sediment-rich overland flow can trigger a debris flow when it reaches an accumulation of coarse debris, either by (partly) saturating the debris or by superimposing a load.

Rainfall intensity, rainfall duration and the infiltration characteristics of the regolith determine whether or not overland flow occurs. The infiltration capacity of a regolith depends on the sorptivity and steady-state infiltration capacity. Cumulative infiltration I is given by

$$I = St^{\frac{1}{2}} + Kt \tag{2}$$

where $t$ = time (T), $S$ = sorptivity ($L T^{-\frac{1}{2}}$) and $K$ = steady-state infiltration capacity ($L T^{-1}$).

$K$ is usually a little less than the saturated hydraulic conductivity $K_{sat}$. This is caused by the enclosure of air bubbles during infiltration. In practice, $K_{sat}$ is often used instead of $K$. This is known as Philips' (1957) mass infiltration equation for ponded infiltration. After differentiation the infiltration capacity $i$ is obtained

$$i = \frac{1}{2}St^{-\frac{1}{2}} + K \tag{3}$$

This equation shows that the infiltration capacity is a monotonically decreasing function with time and that sorptivity is dominant during the initial phase of infiltration (Dunin, 1976). Green and Ampt (1911) developed an analytical solution for infiltration based on the decrease of the hydraulic gradient with time during infiltration. From their solution it appears that sorptivity physically represents the absorption of water by regolith. Sorptivity decreases with increasing (initial) water content of the regolith.

Assuming a constant rainfall intensity, two situations can be distinguished. If the steady-state infiltration capacity exceeds the rainfall intensity, no infiltration excess overland flow will take place. If the rainfall intensity exceeds the steady-state infiltration capacity, initially the infiltration rate will equal the rainfall intensity. At a certain moment ($t_p$), the decreasing infiltration capacity will equal the rainfall intensity and ponding of water at the surface will commence. This moment is therefore called the time to ponding. For $t \geqslant t_p$ the infiltration rate equals the monotonically decreasing infiltration capacity. As this is less than the rainfall intensity, infiltration excess overland flow will occur. Overland flow intensity $i_{of}$ is given by

$$i_{of} = i_r - i \tag{4}$$

The timing of $t_p$ depends on rainfall intensity: $t_p$ increases with decreasing rainfall intensity. The curve showing the relation between time to ponding and rainfall intensity is called the infiltration envelope (see Figure 2). The infiltration envelope approaches $K$ for $t \to \infty$. A well-known function describing the

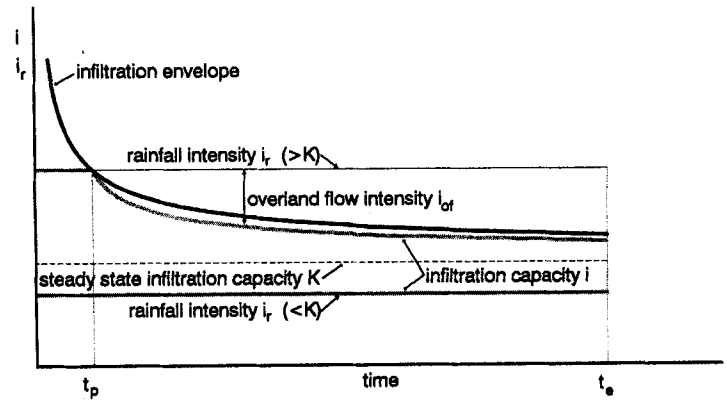


Figure 2. Infiltration envelope and infiltration curves

infiltration envelope is that of Smith and Parlange (1978)

$$\int_0^{t_p} i_r dt = \frac{S^2}{2K} \ln\left(\frac{i_r}{i_r - K}\right) \tag{5}$$

where $\int_0^{t_p} i_r dt$ is the total amount of rainfall until the time to ponding (L).

Another infiltration envelope equation can be derived using Philip's (1957) equations, Equations (2) and (3). The following assumptions are used: (1) the infiltration capacity depends on the total amount of infiltrated water, found from $I = t_p \cdot i_r$; (2) infiltration takes place under non-ponded conditions with a constant infiltration rate equal to the rainfall intensity $i_r$, with $i_r > K$.

From the first assumption it follows that during ponded infiltration $i = i_r$ at $t_* < t_p$. $t_*$ can be calculated from Equation (3)

$$t_* = \frac{S^2}{4(i - K)^2} = \frac{S^2}{4(i_r - K)^2} \tag{6}$$

Combining equations (2) and (6) with the second assumption gives $t_p$

$$t_p = \frac{I}{i_r} = \frac{St_*^{\frac{1}{2}} + Kt_*}{i_r} = \frac{S^2\left(i_r - \frac{K}{2}\right)}{2i_r(i_r - K)^2} \tag{7}$$

which is the 'Philip' infiltration envelope function.

## STUDY AREA

The study was carried out in the Bachelard Valley (Figure 1) in the southern French Alps. The study area is situated between 1120 and 3050 m asl. Rocks in the area are of sedimentary origin. The rock types include limestones, sandstones, conglomerates, marls, schists and flysch-type sediments. Human influence has strongly decreased since the 19th century.

The climate has mediterranean and oceanic influences. Precipitation data recorded at St Laurent (1660m) show a yearly precipitation total of 977 mm, with a maximum in autumn and a secondary maximum in June. Orographic influences cause an increase in precipitation with altitude. In summer and early autumn precipitation often takes the form of short-duration, high-intensity rain storms. For the southern French Prealps, 100 km to the west, Descroix (1989) reports a maximum five-minute rainfall intensity of 64 mm/h during a one year measurement period. Van Asch and Van Steijn (1991) report that debris flows in the Bachelard valley occur at rainfall intensities of 50–100 mm/h over 5–10 minutes.

Debris flow source areas in the Bachelard Valley are located between 2000 and 2800 m asl. They are often found in places with a rapid alternation of weak and resistant rocks. Other source area characteristics include steep slopes, steep gullies or drainage channels and little vegetation cover. Van Steijn (1991) reports slope angles of 33° minimum and 38° mean, drainage channel gradients of at least 30° and less than 10% vegetation cover. Slopes within the source areas consist of bedrock, sometimes covered with a mantle of relatively fine regolith.

## METHODS

Rainfall simulations were carried out in several debris flow source areas to assess the infiltration characteristics of these areas. A rainfall simulator was used rather than taking samples to the laboratory for testing, thus causing little or no damage to the regolith.

The rainfall simulator shown in Figure 3 covers a square horizontal surface of $0{\cdot}060 \pm 0{\cdot}002\,m^2$. Rain is produced from 49 holes on a square grid with 3·5 cm interhole distance. The rainfall simulator is mounted on a frame connected to four rods. The fall height of the raindrops is small, 1·00–1·20 m.

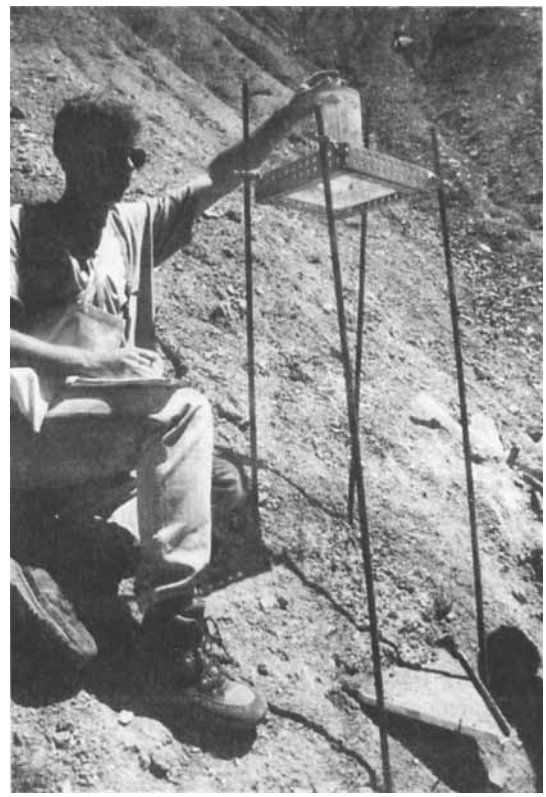

Figure 3. The rainfall simulator

The rainfall simulator produces uniform, large raindrops, compared with raindrops occurring in natural rainfall. To bypass these disadvantages, Imeson (1977) used a rainfall simulator with a larger fall distance and wire-netting to obtain a more realistic raindrop size distribution. However, such improvements would have decreased the practicability of the simulator on the steep slopes.

The rainfall intensity of the simulator can be changed by adjusting the level of an air-entry tube in the simulator. The minimum rainfall intensity of this simulator is about 130 mm/h. As it was expected that the actual rainfall intensities would rarely exceed 100 mm/h, the simulator was modified in 1991 to produce minimum rainfall intensities of 25–30 mm/h.

With each simulation, the mean slope gradient of the test plot, the rainfall intensity $i_r$ and the time to ponding $t_p$ were measured, and the surface type (rill or interrill) and initial wetness were noted. Rainfall intensity was held constant during a simulation. During a 'constant runoff' test the simulation was continued until the overland flow intensity $i_{of}$ became constant. A detailed description of the rainfall simulator and its operation is given by De Graaf *et al.* (1993).

Two different evaluation methods were used. With the 'infiltration envelope' (IE) method, infiltration envelopes were constructed by plotting the time to ponding as a function of rainfall intensity (Imeson and Kwaad, 1982). In the 'constant runoff' (CR) method, $K$ values were calculated from Equation (4) assuming $K \approx i$ when $i_{of}$ became constant. $S$ can then be calculated in several ways.

The CR method involves more actions in the field, making it more sensitive to operational errors than the IE method. Other disadvantages of the CR method are the larger amount of water needed for each test and the larger loss of water by splash. On the other hand, with the CR method $K$ and $S$ values are obtained from each test, whereas with the IE method at least about 10 tests are needed to obtain one $K$ and one $S$ value. Thus the CR method makes it possible to obtain $K$ and $S$ distributions.

## FIELD OBSERVATIONS

Observations in some debris flow source areas have revealed the most important processes at work in these areas. These are overland flow, water erosion and mass movements such as solifluction.

Solifluction occurs mainly during the snowmelt period in spring and has a smoothing effect on the regolith surface, leaving only a few shallow rills at the end of spring. Some micro-scale debris slides up to about 0·5 m long and wide occur on the slopes, mainly under wet conditions.

In summer and early autumn high-intensity rain storms the cause severe erosion of the regolith. During heavy rain storms the existing rills and gullies become deeper and new rills are formed. At the end of summer rills of up to 20 cm deep and wide are abundant on the slopes. Overland flow produced during these rain storms is responsible for these erosion phenomena, as video camera recordings have shown.

During rainfall simulations, some of the above-mentioned processes have also been observed. The initially dry regolith surface is usually irregular, showing a more or less pronounced micro-relief formed by small lumps and fissures. After a dry period, the desiccated top layer of the regolith often forms a crust cemented by lime.

When rainfall starts, the crust softens very quickly, usually within seconds. Raindrops falling on the surface cause splash, which transports material downslope. The splashed material often disappears from the test plot, causing a net loss of water. After some time ponding occurs. The steep slopes offer little opportunity for real ponding, so overland flow begins quickly after the start of ponding. The overland flow immediately concentrates in micro-rills of only a few millimetres wide and deep.

At high rainfall intensities, typically 100 mm/h or more, a remarkable phenomenon sometimes occurs. Within a few minutes after the occurrence of ponding, failure of the top layer of the regolith occurs and

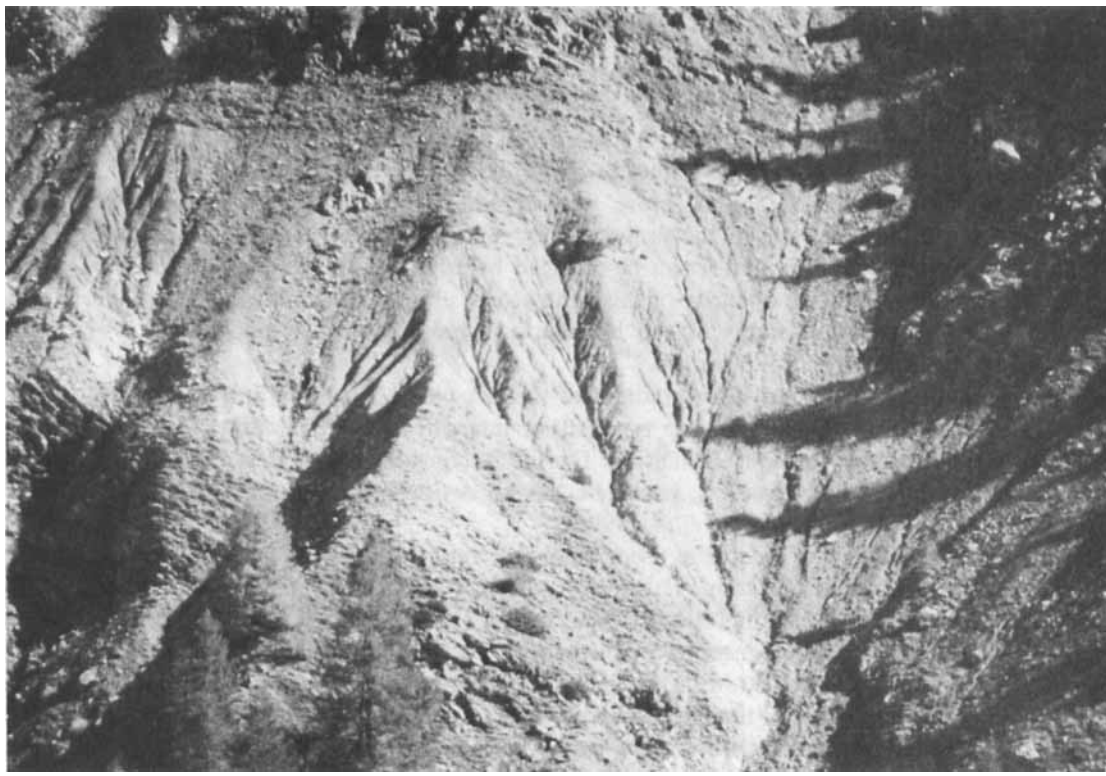

Figure 4. Debris flow source area Tête du Clot des Pastres (TCP)

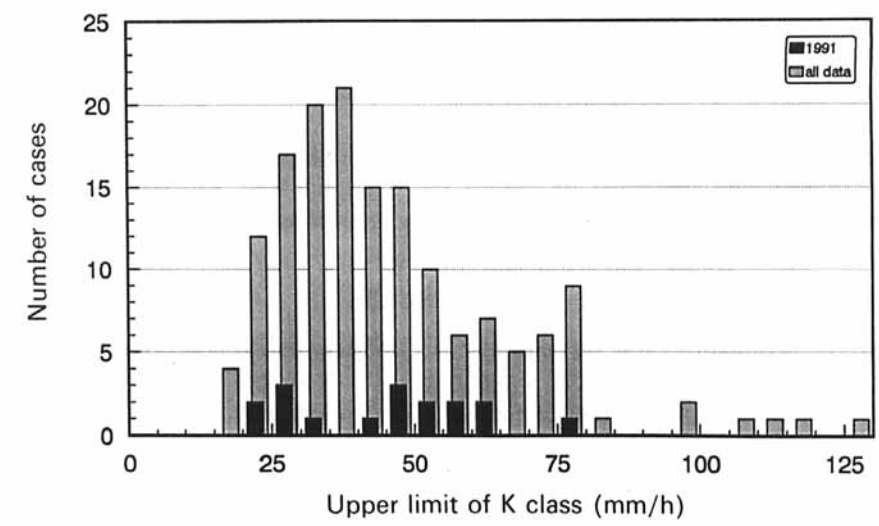


Figure 5. Distribution of $K$ values from the constant runoff method, all data

Table I. $K$ values (mm/h) obtained from rainfall simulations

| | Constant runoff | | Infiltration envelope | |
|---|---|---|---|---|
| | $N$* | $K$ | $N$* | $K$ |
| All data | 154 | 42·1 | | |
| 1990 | 16 | 68·3 | | |
| 1991 | 17 | 41·7 | | |
| 1992 | 126 | 40·4 | | |
| LL, 1990 | 3 | 87·5 | 5 | 131·0 |
| PBN, 1990 | 2 | 53·0 | 10 | 127·1 |
| PBS, 1991 | | | 36 | 51·7 |
| BB, 1991, test series 8 | | | 14 | 40·2 |
| CM, 1992 | 30 | 34·7 | 30 | 47·9 |
| TCP, 1990–1992 | 119 | 43·2 | 221 | 55·9 |
| TCP + PBN + PBS | 121 | 43·3 | 267 | 52·4 |
| TCP, 1990 | 6 | 65·7 | 30 | —† |
| TCP, 1991 | 17 | 41·7 | 82 | 53·0 |
| TCP, 1992 | 96 | 42·3 | 109 | 71·2 |
| TCP, 1990/1991 | 23 | 46·9 | 112 | 45·7 |
| TCP, 1991/1992 | 113 | 42·2 | 191 | 52·3 |
| TCP, 1991, test series 1 | | | 14 | 29·9 |
| TCP, 1991, test series 2 | | | 11 | 45·7 |
| TCP, 1991, test series 3 | | | 14 | 45·9 |
| TCP, 1991, test series 4 | | | 14 | 9·8 |
| PBS, 1991, test series 5 | | | 12 | 67·9 |
| PBS, 1991, test series 6 | | | 12 | 57·4 |
| PBS, 1991, test series 7 | | | 12 | 42·5 |
| Test-plot | 3 | 41·5 | | |

* Number of cases.
† Invalid negative value obtained.

a micro-scale mass movement occurs with dimensions usually $\leqslant 10$ cm long and wide and a few centimetres deep. It usually occurs on a local steepening of the micro-relief. During downslope movement the slide disintegrates and, if it reaches a rill, transforms into a micro-scale debris flow which can move well outside the test plot.

When the rainfall simulation continues after the occurrence of a micro-scale mass movement, the surface usually becomes increasingly smoothed by splash and overland flow. Process dynamics at the surface decrease and no more mass movement occurs during the later phases of a simulation.

## TEST RESULTS

A total of 351 rainfall simulations was carried out in six different debris flow source areas (Figure 1): Tête du Clot des Pastres (further called TCP; 252 simulations); Pra Bouréou North (PBN; 10 simulations); Pra Bouréou South (PBS; 36 simulations); Les Longs (LL; six simulations); Bayasse/Bachelard (BB; 14 simulations); and Combal du Menon (CM; 33 simulations). These simulations were performed in 1990, 1991 and 1992. The test plots had slopes of 27–54°. Rainfall intensities used in the simulations varied from 28 to 291 mm/h.

Most of the simulations were carried out at the TCP site, mainly because this site was chosen as the key monitoring site for the project. The monitoring equipment at this site included rainfall gauges, discharge gauges, a video camera and erosion pins. Figure 4 shows the TCP site, which is located at 2000–2100 m asl on the western slope of the Tête du Clot des Pastres.

### *Constant run-off tests*

*Steady-state infiltration capacity.* The CR method was used in 154 rainfall simulations at TCP, PBN, LL and CM. The slope angles of the test plots ranged from 27 to 52° and rainfall intensities of 55–230 mm/h were used. Individual $K$ values ranged from 17 to 128 mm/h. The data are log-normally distributed, as Figure 5 shows for the overall distribution of $K$ values. The main exception is formed by the 1991 data. Log-mean $K$ values from these tests are presented in Table I.

In Table I regolith types from different parent materials are represented by their locations. It was assumed that different regolith types would have different infiltration characteristics. This assumption was tested by comparing location $K$ distributions in a Student's $t$-test. Table II presents the significance levels for differences in log-mean $K$ values between locations. Bold values indicate significant differences at a 95% confidence level ($p \leqslant 0{\cdot}05$). CM differs from all other locations. PBN does not show a significant difference from TCP. As the parent material at these two sites is the same, this is to be expected. On the other hand, although LL differs significantly from TCP, it has no significant difference with PBN. Here the small number of CR tests at LL and PBN is the main cause for the lack of significance.

Table II. Significance levels for differences in log-mean $K$ values ($K$ values from the CR method)

| | $N$* | CM 1992 | LL 1990 | PBN 1990 | TCP 1990–1992 | TCP 1992 | TCP 1991 | TCP 1990 |
|---|---|---|---|---|---|---|---|---|
| TCP, 1990/1991 | 23 | **0·002**† | **0·028** | 0·718 | 0·294 | 0·318 | 0·397 | 0·107 |
| TCP, 1990 | 6 | **0·000** | 0·292 | 0·478 | **0·016** | **0·019** | **0·029** | |
| TCP, 1991 | 17 | **0·049** | **0·008** | 0·452 | 0·906 | 0·892 | | |
| TCP, 1992 | 96 | **0·019** | **0·006** | 0·553 | 0·969 | | | |
| TCP, 1990–1992 | 119 | **0·010** | **0·007** | 0·518 | | | | |
| PBN, 1990 | 2 | **0·015** | 0·202 | | | | | |
| LL, 1990 | 3 | **0·000** | | | | | | |
| CM, 1992 | 30 | | | | | | | |

* Number of cases.

† Bold values indicate significant difference at the $p = 0{\cdot}05$ (95% confidence) level.

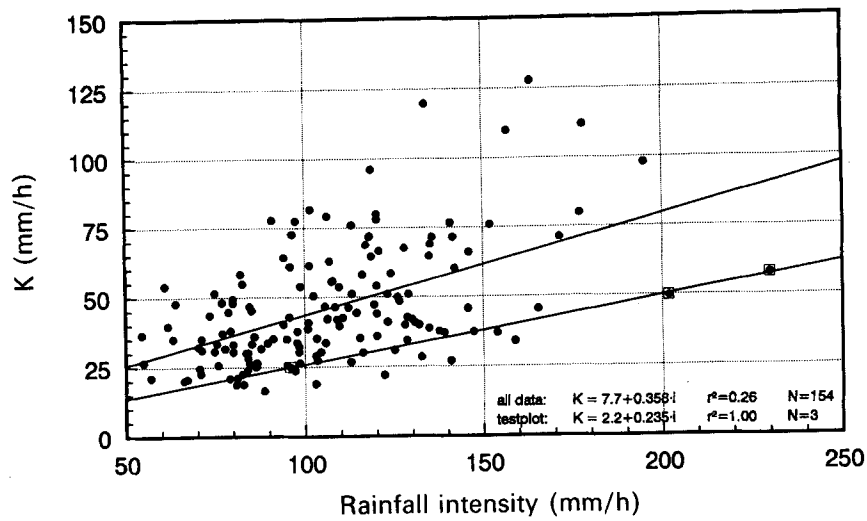


Figure 6. Relation between $K$ and rainfall intensity

$K$ values from the TCP site in 1990 show a significant difference from those of 1991 and 1992. This is probably caused by the high rainfall intensities used in the 1990 simulations, as $K$ values appear to be influenced by rainfall intensity (see Figure 6). The mean rainfall intensity used in 1990 was 144 mm/h, whereas in 1991 and 1992 it was about 105 mm/h. The test plot data from Figure 6 were obtained by testing one plot with three different rainfall intensities. It shows a strong linear relation between $K$ and rainfall intensity. The increase of $K$ with $i_r$ could result from several causes.

1. The 'constant runoff' intensity increases with rainfall intensity, causing a greater depth of the water film at the surface and an increased hydraulic head between the surface and the wetting front. If the wetting front depth is 30 mm, an increase in the water film depth at the surface from 1 to 2 mm results in a 3% higher hydraulic head if only gravity and the water film pressure are considered and even less if matric suction is also considered.
2. A greater depth of the water layer at the surface results in a greater depth of the saturated zone in the regolith immediately below the surface. Therefore more (macro)pores are filled with water and $K$ increases. This means that $K$ is not a constant, but a function of rainfall intensity.
3. Part of the overland flow was not captured due to the imperfect contact of the collection funnel and the regolith surface. This means that measured $K$ values are overestimated. It seems probable that in addition to large random variations, the overland flow loss will increase with increasing overland flow intensity and thus with increasing rainfall intensity.
4. Splash loss is a significant factor in the apparent relation between $K$ and $i_r$. In natural rainfall the net loss by splash is zero, but due to the small size of the test plots a fraction of the rainfall splashes outside the plot in simulations. If each raindrop causes a constant fraction, $c$, to splash outside the test plot, the splash loss increases linearly with rainfall intensity. Corrected $K$ values $K'$ can then be calculated from

$$K' = (i_r - i_s) - i_{of} = (i_r - i_{of}) - i_s = K - ci_r \tag{8}$$

where $i_s$ = splash loss intensity (mm/h).

Assuming that splash loss is the dominant factor determining the relation between $K$ and $i_r$, Equation (8) can be used to assess the amount of splash loss and to correct the measured rainfall intensities and $K$ values. Correcting the test plot data from Figure 6 decreases the log-mean $K$ value from 41·5 mm/h (at $i_r = 167$ mm/h) to 2·2 mm/h (at $i_r = 0$ mm/h). In some instances, the correction of individual $K$

Table III. Sorptivity values (cm/min$^{\frac{1}{2}}$) obtained from different evaluation methods

| | Constant runoff | | | | | Infiltration envelope | |
|---|---|---|---|---|---|---|---|
| | Direct | $t_p$–$F_{S\&P}$ plot | | $t_p^{\frac{1}{2}}$–$F_{S\&P}^{\frac{1}{2}}$ plot | | Philip | Smith and Parlange |
| | | All data | Outliers rejected | All data | Outliers rejected | | |
| All data | 0·194 | 0·183 | 0·169 | 0·181 | 0·176 | | |
| 1990 | 0·224 | 0·210 | 0·210 | 0·213 | 0·213 | | |
| 1991 | 0·206 | 0·200 | 0·162 | 0·195 | 0·171 | | |
| 1992 | 0·190 | 0·174 | 0·170 | 0·177 | 0·175 | | |
| LL, 1990 | 0·327 | | | | | | |
| PBN, 1990 | 0·189 | | | | | | |
| PBS, 1991 | | | | | | 0·20 | 0·27 |
| BB, 1991, test series 8 | | | | | | 0·25 | 0·32 |
| CM, 1992 | 0·226 | 0·207 | 0·207 | 0·215 | 0·215 | 0·17 | 0·21 |
| TCP, 1990–1992 | 0·183 | 0·178 | 0·160 | 0·173 | 0·165 | 0·14 | 0·20 |
| TCP + PBN + PBS | 0·183 | 0·178 | 0·159 | 0·173 | 0·165 | 0·15 | 0·22 |
| TCP, 1990 | 0·196 | 0·204 | 0·204 | 0·201 | 0·201 | | |
| TCP, 1991 | 0·206 | 0·200 | 0·162 | 0·195 | 0·171 | 0·15 | 0·21 |
| TCP, 1992 | 0·179 | 0·162 | 0·158 | 0·166 | 0·163 | 0·14 | 0·20 |
| TCP, 1990/1991 | 0·203 | 0·200 | 0·164 | 0·195 | 0·174 | 0·17 | 0·23 |
| TCP, 1991/1992 | 0·183 | 0·178 | 0·159 | 0·172 | 0·164 | 0·16 | 0·21 |
| TCP, 1991, test series 1 | | | | | | 0·17 | 0·23 |
| TCP, 1991, test series 2 | | | | | | 0·20 | 0·28 |
| TCP, 1991, test series 3 | | | | | | 0·17 | 0·24 |
| TCP, 1991, test series 4 | | | | | | 0·18 | 0·23 |
| PBS, 1991, test series 5 | | | | | | 0·20 | 0·31 |
| PBS, 1991, test series 6 | | | | | | 0·21 | 0·28 |
| PBS, 1991, test series 7 | | | | | | 0·20 | 0·25 |

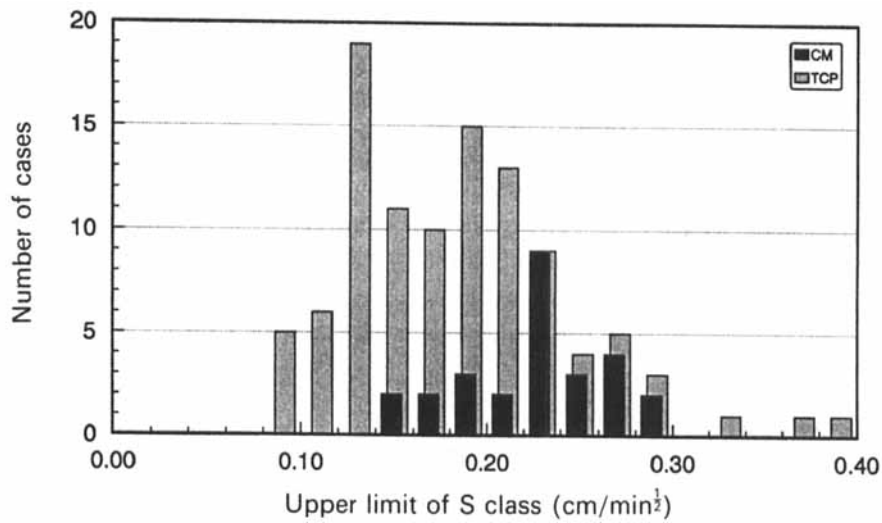


Figure 7. Distribution of $S$ values from the constant runoff 'direct' method, TCP and CM data

Table IV. Significance levels for differences in mean $S$ values ($S$ values from the CR'direct' method)

| *A* | *N** | CM 1992 | LL 1990 | PBN 1990 | TCP 1990–1992 | TCP 1992 | TCP 1991 | TCP 1990 |
|---|---|---|---|---|---|---|---|---|
| TCP, 1990+1991 | 20 | 0.122 | **0.012†** | 0.768 | 0.172 | 0.094 | 0.908 | 0.804 |
| TCP, 1990 | 5 | 0.139 | **0.036** | 0.910 | 0.645 | 0.519 | 0.760 | |
| TCP, 1991 | 15 | 0.207 | **0.023** | 0.750 | 0.178 | 0.104 | | |
| TCP, 1992 | 83 | **0.000** | **0.001** | 0.799 | 0.580 | | | |
| TCP, 1990–1992 | 103 | **0.001** | **0.001** | 0.889 | | | | |
| PBN, 1990 | 2 | 0.248 | 0.239 | | | | | |
| LL, 1990 | 2 | **0.002** | | | | | | |
| CM, 1992 | 27 | | | | | | | |
| *B* | *N** | 1992 | 1991 | 1990 | | | | |
| All data | 134 | 0.600 | 0.487 | 0.167 | | | | |
| 1990 | 9 | 0.107 | 0.554 | | | | | |
| 1991 | 15 | 0.336 | | | | | | |
| 1992 | 110 | | | | | | | |

* Number of cases.

values results in negative $K$ values. Thus splash cannot be the only factor involved in the $K$–$i_r$ relation. As the quantitative effect of each of the factors involved is not known, the data have not been corrected for these factors. Also, the assumption that splash loss increases linearly with rainfall intensity may be wrong.

*Sorptivity*. Table III presents the results of sorptivity determinations. In the 'direct' method, the sorptivities were calculated for each CR test using the Smith and Parlange Equation (5). $S$ varies from 0·088 to 0·381 cm/min$^{\frac{1}{2}}$. Sorptivity distributions appear to be normally distributed, as shown in Figure 7 for TCP and CM. The mean sorptivities for different locations do not show much variation: 0·183–0·226 cm/min$^{\frac{1}{2}}$, except for the significantly higher values at LL. The mean sorptivities at CM are significantly higher than the sorptivities at TCP (see Table IV). Even though only two $S$ values have been obtained at PBN, these values compare well with TCP values. This was expected as both sites have the same regolith parent material.

Two other methods were used to calculate the mean sorptivities from the CR method. These methods are also based on the Smith and Parlange Equation (5). Assuming constant rainfall intensity, this equation can be written as

$$t_p = S^2 F_{S\&P} \tag{9}$$

or

$$t_p^{\frac{1}{2}} = S F_{S\&P}^{\frac{1}{2}} \tag{10}$$

where

$$F_{S\&P} = \frac{\ln\left(\dfrac{i_r}{i_r - K}\right)}{2 i_r K}$$

is the Smith and Parlange factor.

When $t_p$ is plotted as a function of $F_{S\&P}$, the mean sorptivity is the square root of the tangent of the regression line of the data set (Figure 8). For $t_p^{\frac{1}{2}}$ plotted against $F_{S\&P}^{\frac{1}{2}}$, the mean sorptivity is the tangent of

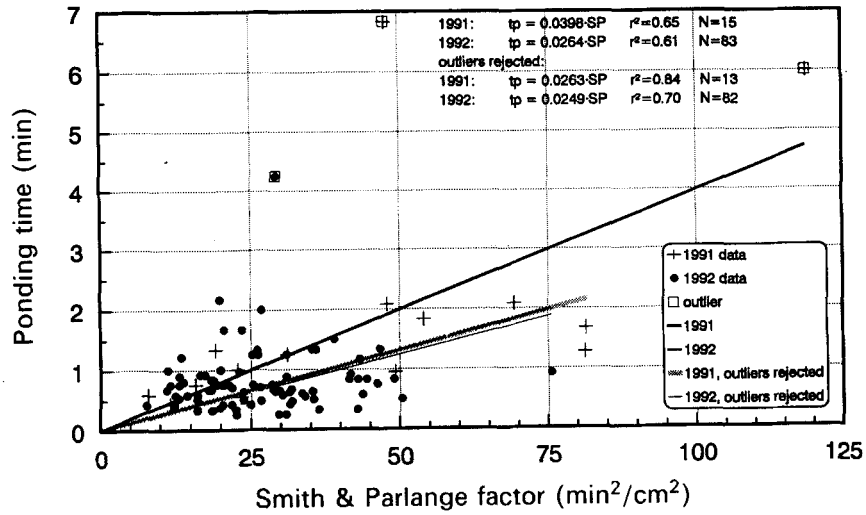


Figure 8. Sorptivity determined from time to ponding – Smith and Parlange factor plot

the regression line. Table III shows that both methods produce very similar $S$ values, with a maximum difference of 3%. Compared with the 'direct' method, these methods give on average 4–5% smaller $S$ values (range −10 to +4%).

Table III shows that outliers have little effect on the mean $S$ value in the CR 'direct' method. Data from CM show no outliers, and rejection of the three outliers at the TCP site will decrease the mean $S$ value with only 3% from 0·183 to 0·178 cm/min$^{\frac{1}{2}}$ (range −6 to 0%). The $t_p^{\frac{1}{2}}$–$F_{S\&P}^{\frac{1}{2}}$ method is slightly more sensitive to a rejection of outliers with an average decrease of 4% (−12 to 0%). The $t_p$–$F_{S\&P}$ method (Figure 8) reacts even more strongly, with an average decrease of 8% (−19 to 0%).

*Relation between steady-state infiltration capacity and sorptivity.* According to Green and Ampt (1911), sorptivity is linearly related to the square root of the steady-state infiltration capacity. Figure 9 shows the relation between $K$ and $S$ for TCP. At a 95% confidence level, the overall data and the 1992 data have significant relations between $K$ and $S$. These relations are not very strong, with only 13–23% of the $S$

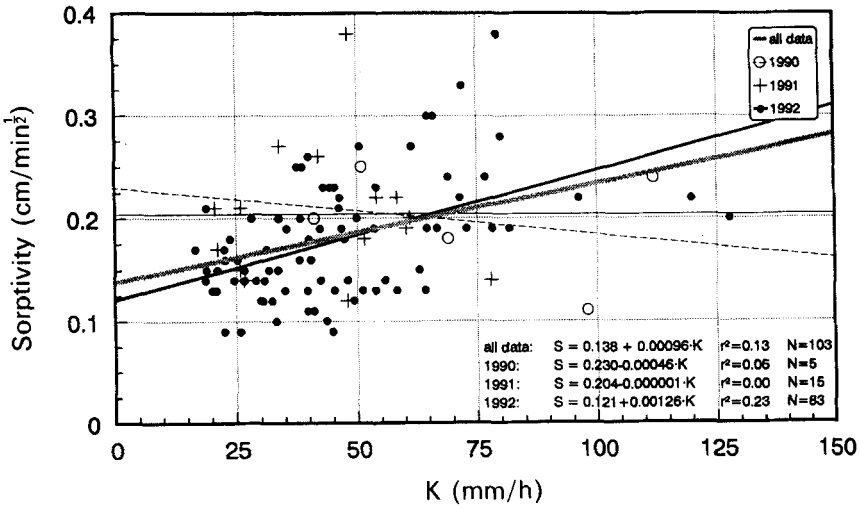


Figure 9. Relation between $K$ and $S$, TCP data

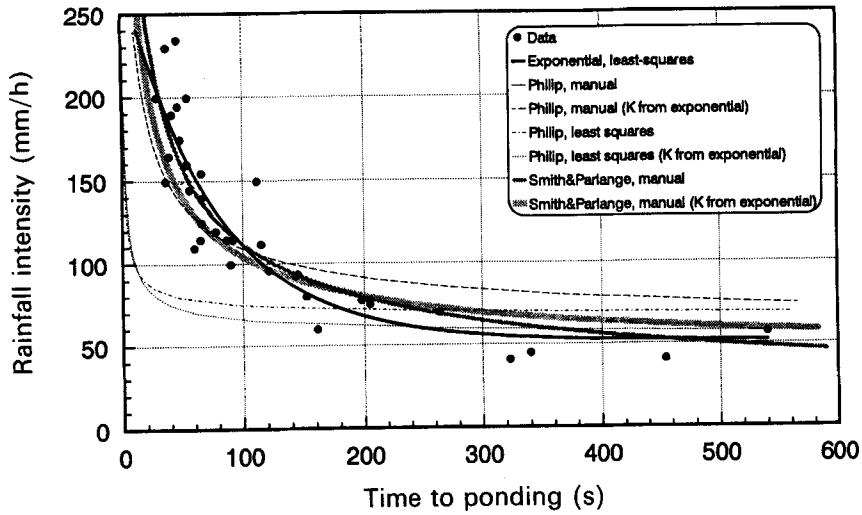


Figure 10. Comparison of infiltration envelope functions and fitting methods, PBS data

variation explained. The 1990 and 1991 data do not show a significant relation. If $S$ is plotted against the square root of $K$, the significance and the explained variation of the relations are nearly the same.

*Infiltration envelopes*

A total of 316 'infiltration envelope' tests was performed at TCP, PBN, PBS, LL, BB and CM. The slope angles of the test plots ranged from 27 to 54° and the rainfall intensities from 28 to 291 mm/h.

Figure 10 illustrates that it is not possible to use least-squares fitting for the Philip and Smith and Parlange functions, which is caused by $t_p$ being a function of $i_r$. Manual fitting of these functions usually resulted in a good fit only for near-zero or negative values of $K$. A negative exponential function describes the data better

$$i_r = K + e^{a+bt_p} \tag{11}$$

where $i_r$, $K$ are in mm/h; $t_p$, the time to ponding, is in seconds; $a$, a constant, is in ln(mm/h); and $b$, a constant, is in ln(mm/h)/s.

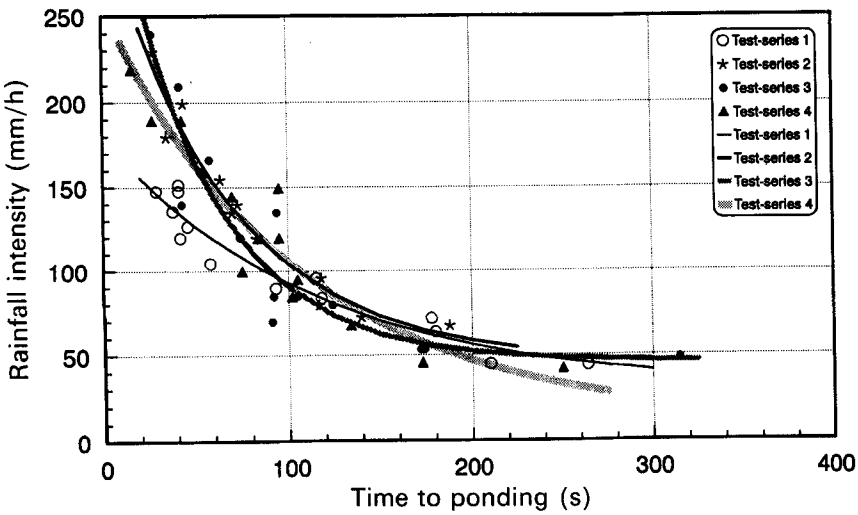


Figure 11. Infiltration envelopes, TCP test series 1–4

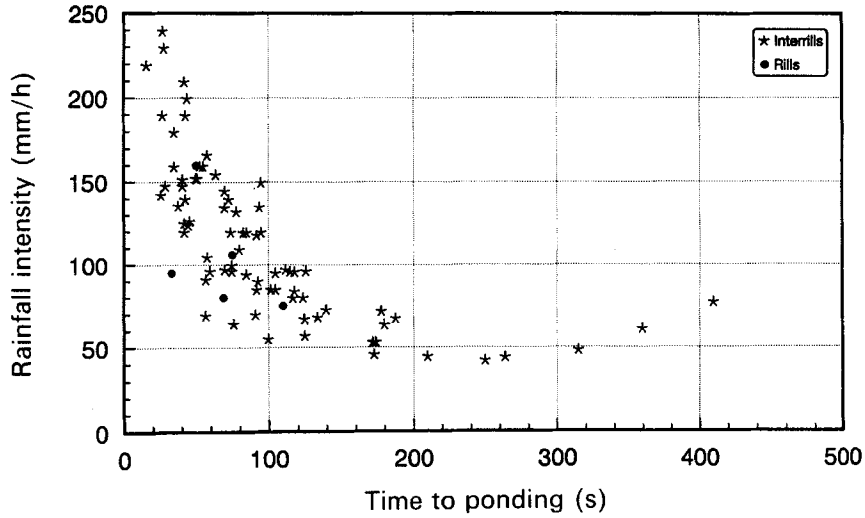


Figure 12. Time to ponding as a function of rainfall intensity for rills and interrill areas, TCP 1991 data

This function explains as much as 87–96% of the variation in $i_r$ for data sets from test plots with similar characteristics (slope angle, regolith type, initial soil wetness, surface type), as shown in Figure 11. The explained variation is far less for less uniform data sets. For data grouped by test location (regolith type) the explained variation ranges from 23 to 92%. Here the high values of explained variation, 82% at Pra Bouréou South and 92% at Bayasse/Bachelard, are again for data sets from test plots which are also similar regarding other characteristics.

*Steady-state infiltration capacity*. The negative exponential function is the only function that produces realistic $K$ values with least-squares fitting. As the physical meaning of the constants $a$ and $b$ in this function is not clear, this function is only used to obtain $K$ values. The results are shown in Table I.

*Sorptivity*. To calculate sorptivities, $K$ values obtained from the negative exponential function were used in the Smith and Parlange and Philip infiltration envelope functions. Table III presents the sorptivities obtained from these methods. The Philip function gives on average 28% lower values than the Smith and Parlange function (19–41% less). The Smith and Parlange function seems to fit the data slightly better than the Philip function.

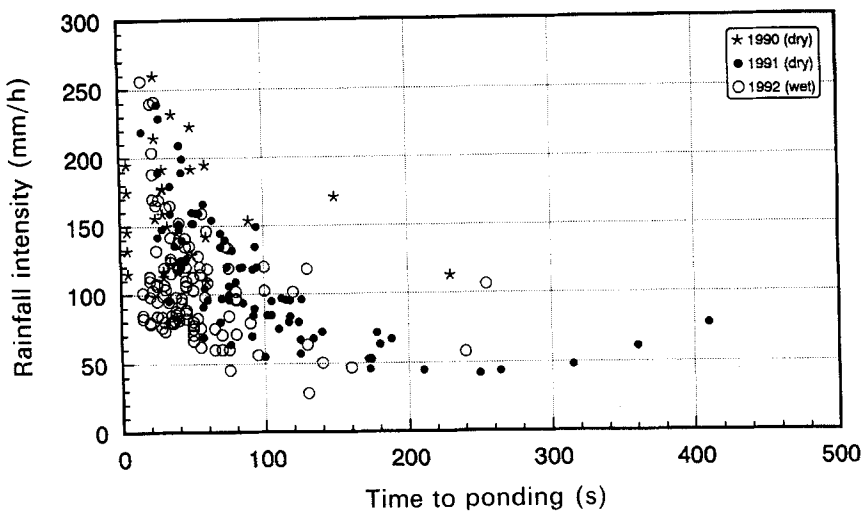


Figure 13. Time to ponding as a function of rainfall intensity and initial soil wetness, TCP data

Figure 14. Micro-scale debris flow during a rainfall simulation

*Effect of surface type and soil wetness on time to ponding.* Figure 12 shows that rills and interrill areas yield the same time to ponding at comparable rainfall intensities. Figure 13 shows that the time to ponding is generally shorter on moist or wet surfaces than on dry surfaces and therefore the sorptivity is generally smaller. The 1992 data in this figure are from a generally wet period and the 1990 and 1991 data are from a dry period.

*Comparison of the test methods*

Table I shows that the CR method gives on average 22% lower $K$ values than the IE method (excluding the LL and PBN data because of the small number of tests at these sites). However, a direct comparison poses some difficulties. When fitting an infiltration envelope, the data points with a large time to ponding have far more influence on the value of $K$ than the data points at smaller times to ponding. This results from the importance of $K$ relative to $S$ in the infiltration envelope functions, which increases with increasing time to ponding. As mentioned earlier, the CR method probably overestimates $K$ values. It then follows that the IE method overestimates $K$ values even more.

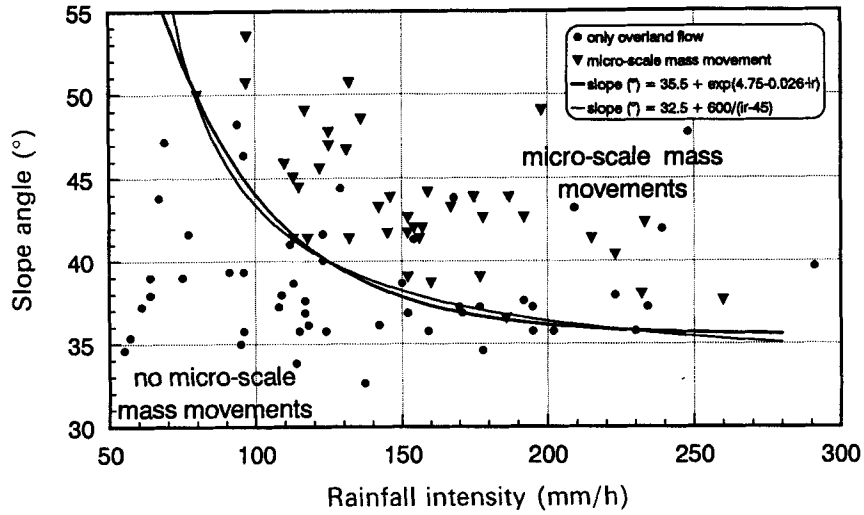


Figure 15. Threshold conditions for the occurrence of micro-scale mass movements during rainfall simulations

As far as sorptivities are concerned, the IE 'Smith and Parlange' method gives the highest values. They are on average 10% higher than values from the CR 'direct' method (−7 to +20%). The IE 'Philip' method gives the lowest values, on average 21% lower than from the CR 'direct method' (−25 to −13%). The three CR methods give similar results.

*Boundary effects during the rainfall simulations*

The plots that are tested during rainfall simulations are not clearly defined in a lateral sense. In the calculations a confined situation is assumed: only vertical flow, caused by gravity and matric forces, occurs in a regolith column beneath the test plot surface (the 'ideal' situation). In reality, the situation is unconfined and matric forces will also cause lateral flow from this column. As water is removed from the column, the wetting front will move downwards slower than in the ideal situation, so $t_p$ will increase compared with the ideal situation. Horizontal flow from the column also implies that for $t \rightarrow \infty$ the infiltration capacity will also be larger than for the ideal situation and therefore the measured value of $K$ will exceed the actual value. At small $t$ values the boundary effects imply that for $S$ the measured values are again higher than the actual values. Quantitative relations between measured and actual values of $t_p$, $K$ and $S$ are still lacking.

*Critical conditions for the initiation of micro-scale mass movements and debris flows*

As mentioned earlier, during some rainfall simulations micro-scale mass movements occurred. Figure 14 shows such a micro-scale debris flow. These mass movements only occurred on steep slopes at high rainfall intensities, with runoff present at the surface. An attempt was made to define the threshold conditions for their occurrence as a function of both slope angle and rainfall intensity. Figure 15 seems to suggest a minimum slope angle of about 34–36° at very high rainfall intensities, and a minimum rainfall intensity (not corrected for splash loss) of about 60–70 mm/h at slope angles of 55° or more. This minimum rainfall intensity must exceed the steady-state infiltration capacity as the occurrence of runoff also seems to be an important factor in the occurrence of the micro-scale mass movements.

These mass movements usually occurred on a local steepening of the micro-relief within the first minutes after ponding. On the other hand, no more mass movement occurred during the later phases of a simulation when the surface became smoothed by runoff and splash. It therefore seems likely that, in addition to the overall slope angle and the rainfall intensity, the surface micro-relief plays an important part in the occurrence of these micro-scale mass movements.

The occurrence of these micro-scale mass movements may be an important link between the occurrence of overland flow and the actual initiation of debris flows. This is supported by eye-witness accounts which

state that debris flows usually occur within 5–10 minutes after the start of high intensity (50–100 mm/h) rainfall (Van Asch and Van Steijn, 1991). The link is probably established through the delivery of high amounts of sediment to the overland flow. This causes an increase in density, viscosity and flow depth of the overland flow, resulting in a higher capacity to mobilize coarse material such as stones.

## CONCLUSIONS

In spite of the disadvantages of the rainfall simulations, the method seems to offer good possibilities for use in difficult terrains. The main advantages are testing on undisturbed material and the relatively quick testing procedure. The main disadvantages are the boundary effects in the soil, water loss by splash and, compared with natural rainfall, the small fall distance and the large, uniform raindrops.

The CR and IE methods both have advantages and disadvantages. In spite of the larger operational difficulties and measurement errors the CR method seems preferable. $K$ and $S$ values are easily calculated, and for each CR test a $K$ and an $S$ value are obtained, making it possible to construct $K$ and $S$ values from multiple CR tests.

The occurrence of micro-scale mass movements at high rainfall intensities on steep slopes seems to be a key factor in the initiation of debris flows. These micro-scale mass movements are likely to deliver high amounts of relatively fine sediment to the overland flow. This sediment-rich overland flow has different hydraulic properties from pure water and has a higher capacity to mobilize coarse material.

### ACKNOWLEDGEMENTS

The project was part of the EPOCH programme of the European Community, which is thanked for providing funds. We also thank Dr van der Perk for his constructive remarks.

### REFERENCES

Bovis, M.J. and Dagg, B.R. 1987. 'Mechanisms of debris supply to steep channels along Howe Sound, southwest British Columbia' in *Erosion and Sedimentation in the Pacific Rim, Proceedings of the Corvallis Symposium (August 1987) IAHS Pub.*, **165**, 191–200.

Brunsden, D. 1979. 'Mass movements' in Embleton, C.E. and Thornes, J.B. (Eds), *Process in Geomorphology*. Arnold, London. pp. 130–186.

Caine, N. 1980. 'The rainfall intensity–duration control of shallow landslides and debris flows', *Geogr. Ann.*, **62-A**, 23–27.

Costa, J.E. 1984. 'Physical geomorphology of debris flows' in Costa, J.E. and Fleisher, P.J. (Eds), *Developments and Applications of Geomorphology*. Springer Verlag, Berlin/Heidelberg. pp. 268–317.

De Graaf, P.J., de Ruiter, J.F., and van Tetering, A.A.A. 1993. 'De initiatie van puinstromen. Een onderzoek in het Bachelarddal, Alpes de Haute-Provence, Frankrijk', *Unpublished Report Utrecht University*, Department of Physical Geography, 119 pp [in Dutch].

Descroix, L. 1989. 'La mesure de l'érosion actuelle dans les terres noires des Preälpes du Sud: recherches sur petites parcelles expérimentales', *Bull. Lab. Rhodanienne Géomorphol.*, **23–24**, 11–29.

Dunin, F.X. 1976. 'Infiltration: its simulation for field conditions' in Rodda, J.C. (Ed.), *Facets of Hydrology*. Wiley, London. pp. 199–227.

Green, W.H. and Ampt, G.A. 1911. 'Studies on soil physics. Part I: the flow of water and air through soils', *J. Agric. Sci.*, **4**, 1–24.

Imeson, A.C. 1977. 'A simple field portable rainfall simulator for difficult terrain', *Earth Surf. Process.*, **2**, 431–436.

Imeson, A.C. and Kwaad, F.J.P.M. 1982. 'Field measurements of infiltration in the Rif Mountains of Northern Morocco', *Stud. Geomorphol. Carpatho-Balcanica*, **15**, 19–30.

Innes, J.L. 1983. 'Debris flows', *Prog. Phys. Geogr.*, **7–4**, 469–501.

Johnson, A.M. and Rahn, P.H. 1970. 'Mobilization of debris flows', *Z. Geomorphol., Suppl.* **9**, 168–186.

Johnson, A.M. and Rodine, J.R. 1984. 'Debris flow' in Brunsden, D. and Prior, D.B. (Eds), *Slope Instability*. Wiley, London. pp. 257–361.

Philip, J.R. 1957. 'The theory of infiltration. I. The infiltration equation and its solution', Soil Sci., **83**, 345–357.

Smith, R.E. and Parlange, J.Y. 1978. 'A parameter-efficient hydrologic infiltration model', *Wat. Resour. Res.*, **14**, 533–538.

Takahashi, T. 1978. 'Mechanical characteristics of debris flow', *J. Hydr. Div. Proc. ASCE*, **104-HY8**, 1153–1169.

Takahashi, T. 1980. 'Debris flow on prismatic open channel', *J. Hydr. Div. Proc. ASCE*, **106-HY3**, 381–396.

Takahashi, T. 1981. 'Debris flow', *Annu. Rev. Fluid Mech.*, **13**, 57–77.

Van Asch, Th.W.J. and Van Steijn, H. 1991. 'Temporal patterns of mass movements in the French Alps', *Catena*, **18-5**, 515–527.

Van Steijn, H. 1991. 'Frequency of hillslope debris flows in a part of the French Alps', *Bull. Geomorphol.*, **19**, 83–90.

Varnes, D.J. 1978. 'Slope movement types and processes' in Schuster, R.L. and Krizek, R.J. (Eds), *Landslides, Analysis and Control Spec. Rep.*, **176**, Transportation Research Board of the National Academy of Sciences, Washington, 11–33.